Quality or Quantity? How Structural Parameters Affect Catalytic Activity of Iron Oxides for CO Oxidation

Steffen Schlicher [1], Nils Prinz [2], Julius Bürger [3], Andreas Omlor [4], Christian Singer [5], Mirijam Zobel [2], Roland Schoch [1], Jörg K. N. Lindner [3], Volker Schünemann [4], Sven Kureti [5] and Matthias Bauer [1,*]

[1] Department of Chemistry and Center for Sustainable Systems Design (CSSD), Paderborn University, Warburger Straße 100, 33098 Paderborn (Germany); Matthias.Bauer@upb.de

[2] Institute of Crystallography, RWTH Aachen University, Jägerstr. 17-19, 52066 Aachen (Germany); Zobel@ifk.rwth-aachen.de

[3] Department of Physics, Paderborn University, Warburger Straße 100, 33098 Paderborn (Germany); Lindner@physik.upb.de

[4] Department of Physics, Technical University of Kaiserslautern, Erwin-Schrödinger-Straße 46, 67663 Kaiserslautern (Germany); Schuene@physik.uni-kl.de
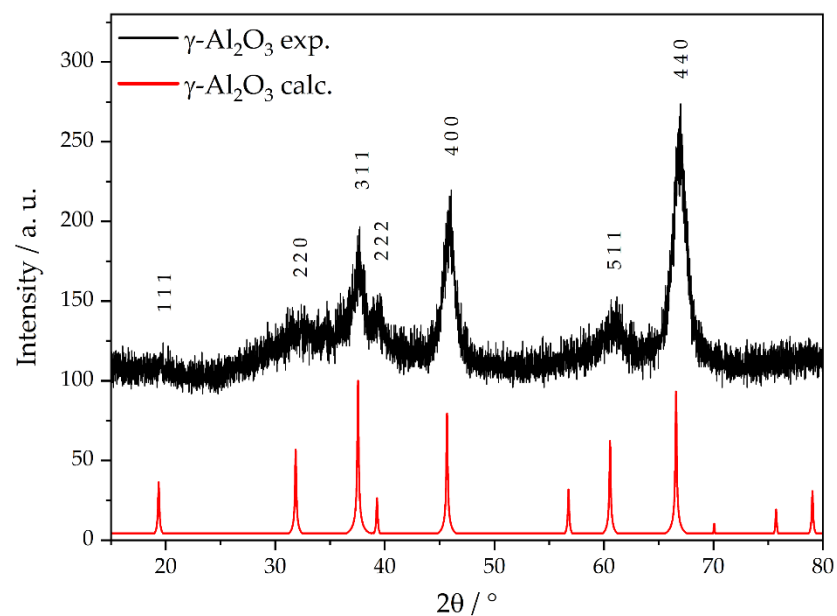
[5] Institute of Energy Process Engineering and Chemical Engineering, Chair of Reaction Engineering, Technical University of Freiberg, Fuchsmühlenweg 9, 09599 Freiberg (Germany); Sven.Kureti@iec.tu-freiberg.de

* Correspondence: Matthias.Bauer@upb.de

Table of Contents

1. Phase Purity of the γ-Al₂O₃ Support

Figure S1.: Experimental powder X-ray diffractogram of the as prepared γ-Al₂O₃ support compared to a calculated powder pattern, obtained via the program Mercury[1] from a crystal structure[2,3].

2. Powder X-Ray Diffraction

Powder X-ray diffractometry was carried out at a Bruker AXS D8 Advance with an incident Cu K$_\alpha$ radiation (λ = 1.54 Å), a step size of 2θ = 0.02°, time per step of 3 s and a wide-angle range of 10° to 80°.
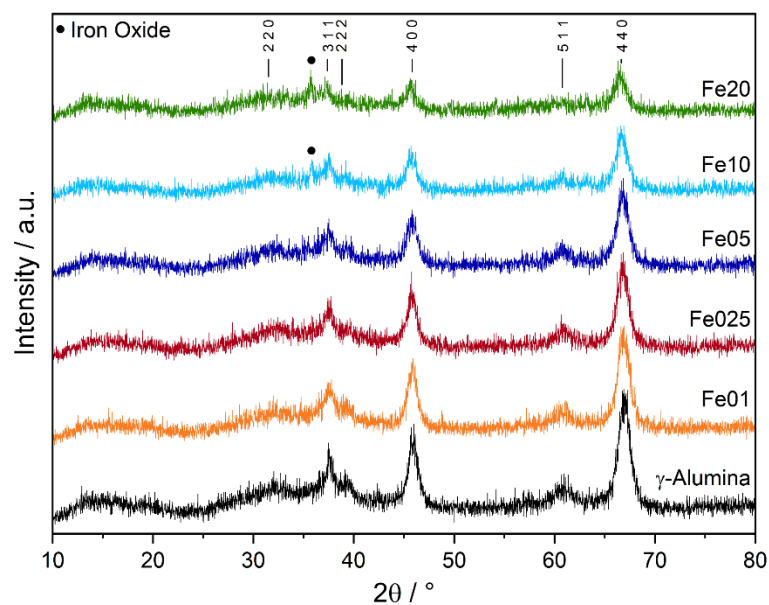
Figure S2. powder X-ray diffractograms of Fe01 to Fe20, compared to the γ-Al$_2$O$_3$ support, obtained at the in-house setup.

3. High Resolution Powder X-Ray Diffraction

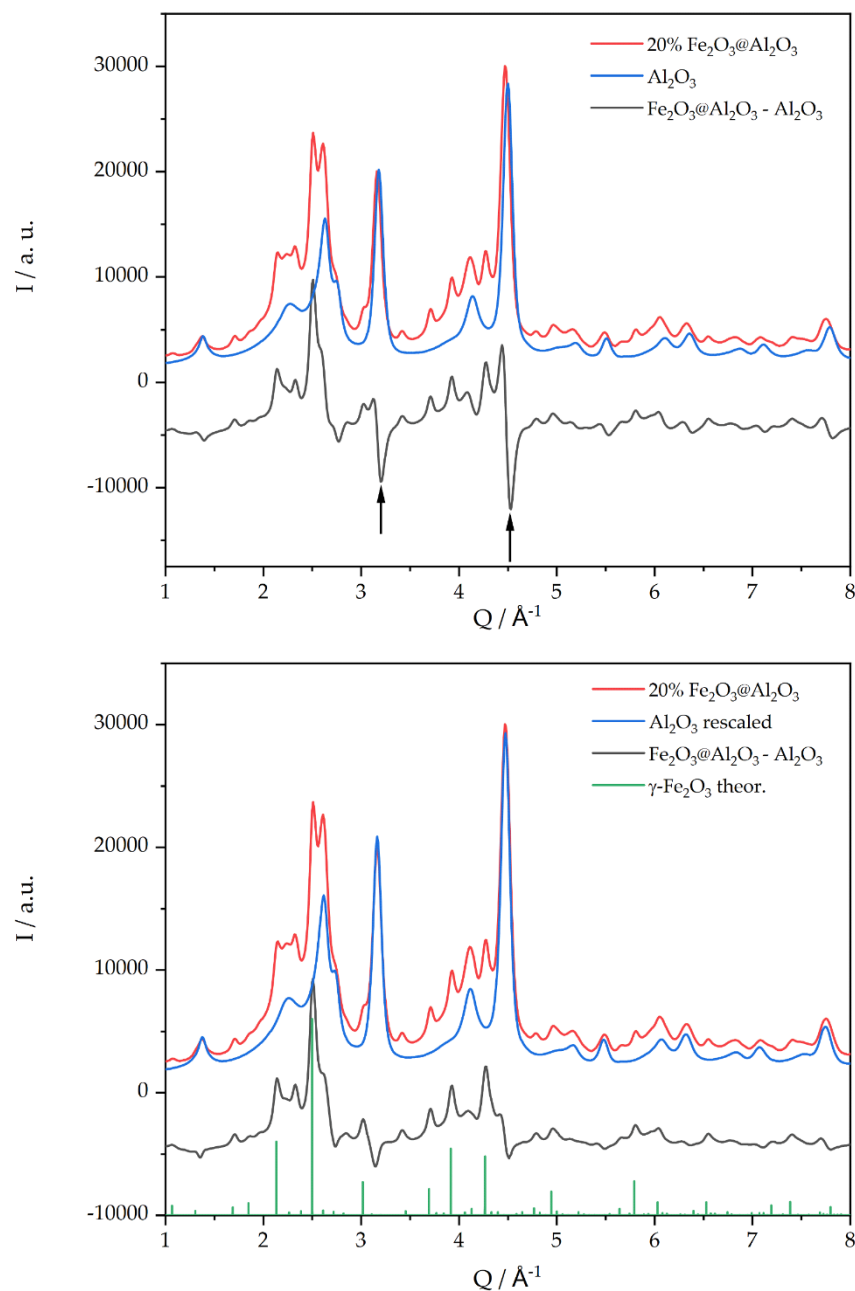Calculation of Plane Distance d and Lattice Parameter a:

According to Bragg´s law the plane distances can be calculated by

$$d = \frac{\lambda}{2 \sin\left(\frac{\theta\pi}{180}\right)} \tag{S1}$$

These parameters can further be transformed into the lattice parameter *a* for each plane using its Miller or Laue indices by the following formula:

$$d = \frac{a}{\sqrt{h^2 + k^2 + l^2}} \tag{S2}$$

4. Pair Distribution Function Analysis

Figure S3: XRD of 20 % Fe loading (red) together with unloaded Al_2O_3 support (blue) and difference curve (grey, in offset). The top panel shows the direct subtraction of experimental data resulting in strong dips at Q values where strong Al_2O_3 reflexes of unloaded support appear, because the modified lattice parameters of the Al_2O_3 are not taken into account. Bottom panel contains the Al_2O_3 pattern compressed by the compressing factor s for a better match of the Al_2O_3 reflexes, thus creating less strong dips in the difference curve, which is indexed with γ-Fe_2O_3.
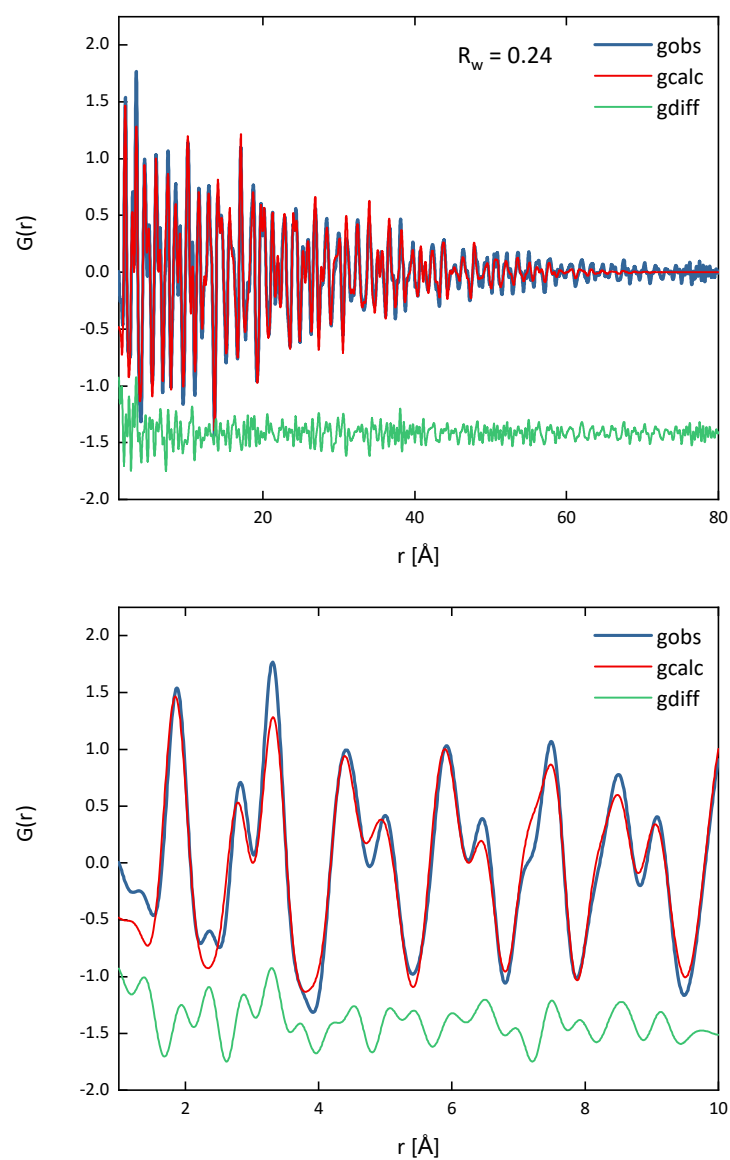
Figure S4: PDF refinement of the γ-Al₂O₃ support over the range 1 - 80 Å (a) and magnification of the 1-10 Å range (b).
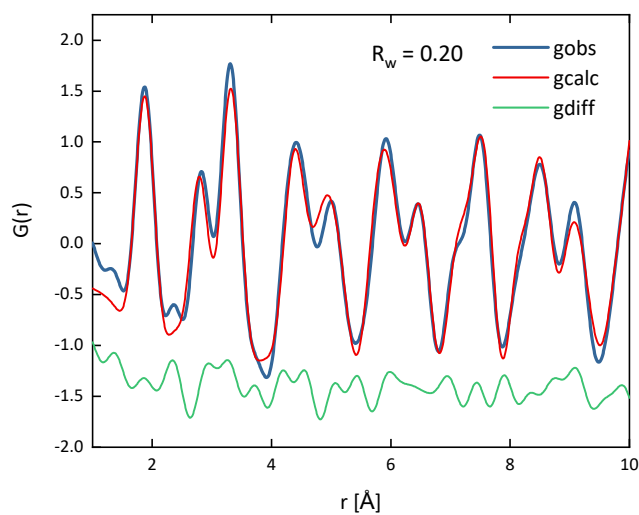
Figure S5: refinement of only the short-range order of the γ-Al_2O_3 support between 1 - 10 Å with different occupation of octahedral and tetrahedral positions.

The nominal occupancies of Al^{3+} ions on tetrahedral (8a, 48f Wyckoff positions) and octahedral positions (16c, 16d Wyckoff positions) were refined to 0.4 and 0.6 respectively. A high fraction of 22% of all Al^{3+} ions occupy non-spinel positions (16c, 48f Wyckoff positions), and these non-spinel positions are needed for a good agreement in the long range.

Table S1. : Refinement values.

Parameter	Range 1–80 Å	Range 1–10 Å
B_{iso} 16c (Al^{3+})	1.6 Å^2	0.01 Å^2
B_{iso}16d (Al^{3+})	0.9 Å^2	0.9 Å^2
B_{iso}48f(Al^{3+})	0.4 Å^2	0.2 Å^2
B_{iso}8a (Al^{3+})	1.7 Å^2	1.0 Å^2
B_{iso} (O^{2-})	2.0 Å^2	2.2 Å^2
Lattice parameter a	7.919 Å	7.927 Å
$\delta2$	2.5	2.3
Occupancy 16c site	0.20	0.08
Occupancy 16d site	0.59	0.74
Occupancy 48f site	0.03	0.04
Occupancy 8a site	0.89	0.77
Calculated nominal occupied octahedral(16c,16d) Al^{3+} positions	0.60	0.62
Nominal fraction of non-spinel positions (16c, 48f)	0.22	0.15
Crystal domain size	7.1 nm	11.9 nm

5. Low Temperature Mössbauer Spectroscopy (77 K)

Fe025:
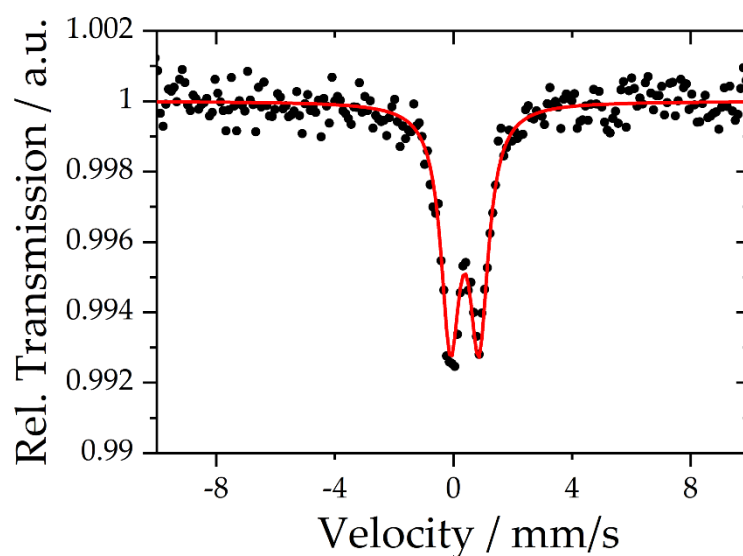
Figure S6: Mössbauer spectrum of Fe025 (black dots) obtained at 77 K and corresponding fit of the doublet (red).

Table S2: Parameters obtained by Mössbauer spectroscopy of Fe025 at 77 K.

δ [mm/s]	ΔE$_Q$ [mm/s]	Γ [mm/s]
0.38	0.97	0.76

Fe05:

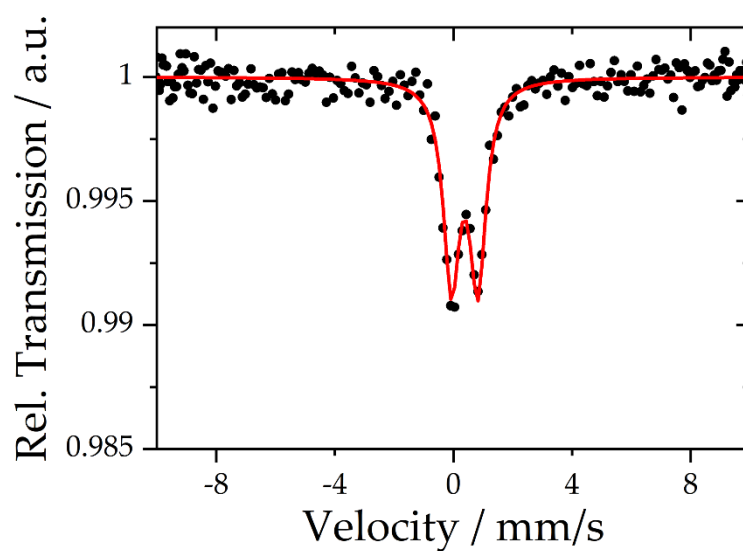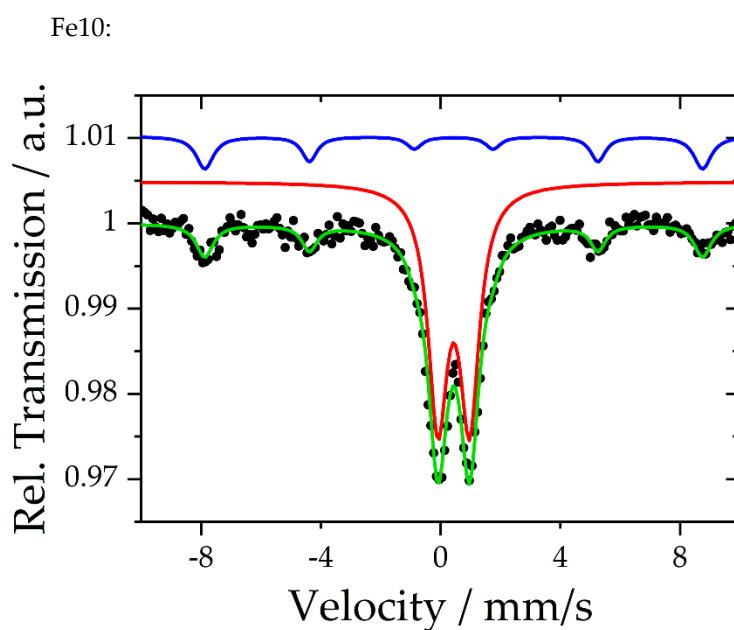**Figure S7:** Mössbauer spectrum of Fe05 (black dots) obtained at 77 K and corresponding fit of the doublet (red).

Table S3: Parameters obtained by Mössbauer spectroscopy of Fe05 at 77 K.

δ [mm/s]	ΔE$_Q$ [mm/s]	Γ [mm/s]
0.38	0.89	0.66

Fe10:

Figure S8: Mössbauer spectrum of Fe10 (black dots) obtained at 77 K, fit of the doublet (red), sextet (blue) and the cumulative fit (green).

Table S4: Parameters obtained by Mössbauer spectroscopy of Fe10 at 77 K. Ratio doublet to sextet 80:20 by area.

	δ [mm/s]	ΔE$_Q$ [mm/s]	Γ [mm/s]
d	0.44	1.06	0.77
sx	0.44	B$_{hf}$ = 51.5 T	

Fe20:

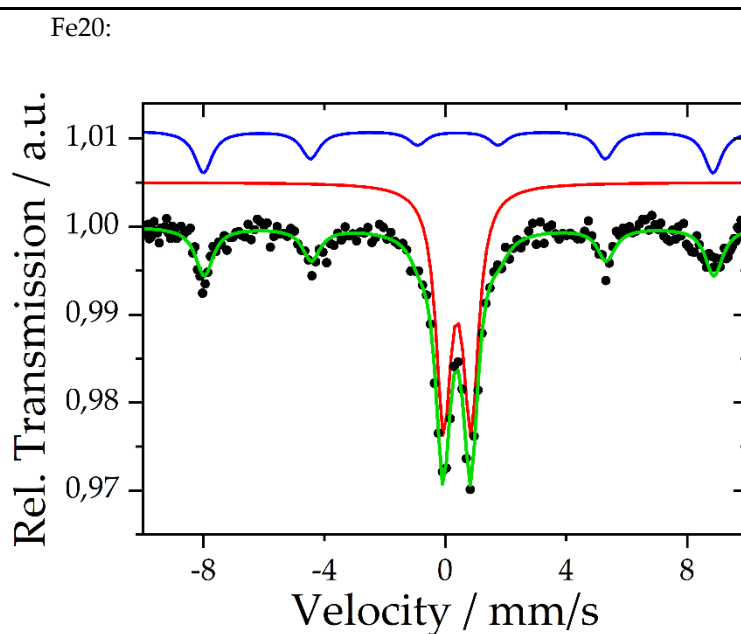**Figure S9:** Mössbauer spectrum of Fe20 (black dots) obtained at 77 K, fit of the doublet (red), sextet (blue) and the cumulative fit (green).

Table S5: Parameters obtained by Mössbauer spectroscopy of Fe20 at 77 K. Ratio doublet to sextet 67:33 by area.

	δ [mm/s]	ΔE$_Q$ [mm/s]	Γ [mm/s]
d	0.39	0.91	0.51

sx	0.46	$B_{hf} = 52.3$ T

6. UV/Vis Spectroscopy

Peak deconvolution of the diffuse reflectance UV/Vis spectra was carried out using the NLFit function of Origin 2020b with 5 Gaussian type functions for catalysts Fe01, Fe025 and Fe05 and with 6 Gaussian type functions for Fe10 and Fe20. The range of the fitted area was kept between the first zero value for absorption in both lower and upper energy direction. The starting points for the peakfit were set manually at 270, 300, 350, 450, 530 and 650 nm matching the visible shoulders/peaks in approximation. The y0 lower limits were set manually for each fit corresponding to the lower limit of the experimental spectra and for peaks 1 and 3 lower limits of 260 nm, respectively 340 nm, were set.

Fe01:
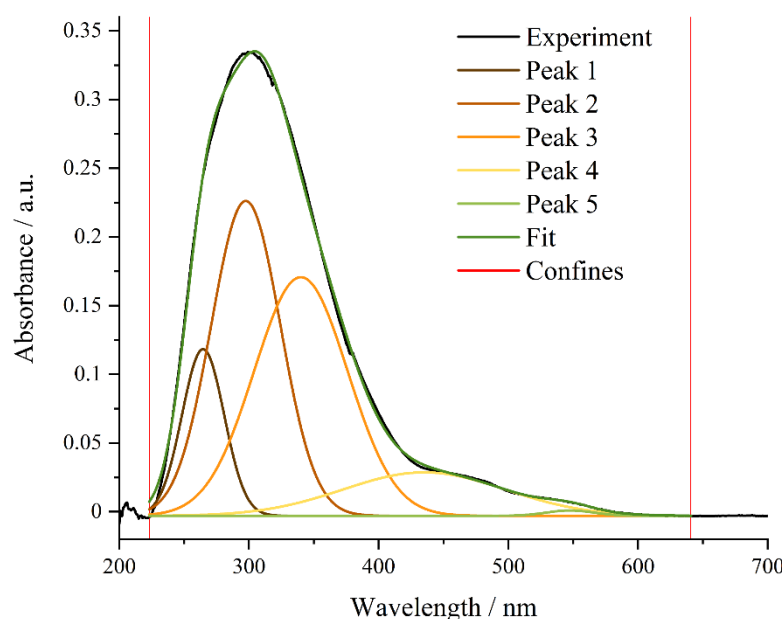
Figure S10: DRUV spectrum and deconvolution of Fe01.

Table S6: Parameters of the peak deconvolution of Fe01.

Model	Gaussian				
Function	$y=y0 + (A/(w*sqrt(pi/2)))*exp(-2*((x-xc)/w)^2)$				
	Peak 1	Peak 2	Peak 3	Peak 4[1]	Peak 5
Y0	$-0.003 \pm 8.19729E-4$	$-0.003 \pm 8.19729E-4$	$-0.003 \pm 8.19729E-4$	$-0.003 \pm 8.19729E-4$	$-0.003 \pm 8.19729E-4$
x_c	264.59438 ± 0.44817	297.54298 ± 1.91962	340 ± 13.18916	435 ± 23.47277	547.55219 ± 4.11191
Area	4.94029 ± 1.17361	15.31479 ± 7.63358	15.70824 ± 8.3174	4.95468 ± 2.16194	0.17939 ± 0.15203
χ^2_{red}	8.64457E-6				
r^2_{corr}	0.99934				

1) For catalyst Fe01 a lower limit of 435 nm was set for peak 4.

Table S7: Assignment of the peaks and their normalized areas to tetrahedral, octahedral and oligomerized iron oxide. Percentual amounts of the respective iron species of the overall amount of catalyst, calculated from the percentual areas multiplied by the iron loading.

X_C [nm]	Area [a.u.]	Area$_{norm}$ [%]	Area$_{norm}$ [%]		Amount$_{norm}$ [wt%]
265	4.94	12.0223899	Fe$_{tet}$	12.0	0.12022
298	15.31	37.2596739	Fe$_{oct}$	37.3	0.3726
340	15.71	38.2331468	Fe$_x$O$_y$ olig.	50.3	0.5028
435	4.95	12.0467267			
548	0.18	0.43806279	Fe$_x$O$_y$ particles	0.44	0.00438

Fe025:

Figure S11: DRUV spectrum and deconvolution of Fe025.

Table S8: Parameters of the peak deconvolution of Fe025.

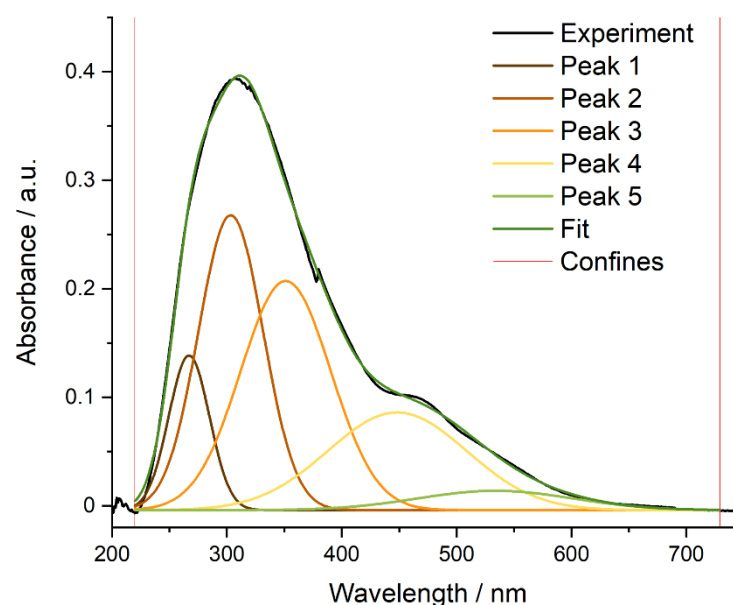| Model	Gaussian				
Function	y=y0 + (A/(w*sqrt(pi/2)))*exp(-2*((x-xc)/w)^2)				
	Peak 1	Peak 2	Peak 3	Peak 4	Peak 5
Y0	-0.004 ± 0.00123	-0.004 ± 0.00123	-0.004 ± 0.00123	-0.004 ± 0.00123	-0.004 ± 0.00123
x_c	267.06786 ± 0.83954	303.37247 ± 1.98923	351.23636 ± 14.88785	448.35421 ± 47.75321	533.71673 ± 475.13726
Area	6.33151 ± 1.96755	19.19314 ± 11.61768	20.79024 ± 15.63306	13.63946 ± 35.64092	3.02486 ± 30.08959
χ^2_{red}	1.27031E-5				
r^2_{corr}	0.99923				

Table S9: Assignment of the peaks and their normalized areas to tetrahedral, octahedral and oligomerized iron oxide. Percentual amounts of the respective iron species of the overall amount of catalyst, calculated from the percentual areas multiplied by the iron loading.

X_C [nm]	Area [a.u.]	Area$_{norm}$ [%]	Area$_{norm}$ [%]		Amount$_{norm}$ [wt%]
267	6.33	10,7891597	Fe$_{tet}$	10.8	0.26973
303	20.79	35,4354866	Fe$_{oct}$	35.4	0.88589
351	14.89	25,3792398	Fe$_x$O$_y$ olig.	48.6	1.2157
448	13.64	23,2486791			
534	3.02	5,1474348	Fe$_x$O$_y$ particles	5.15	0.12869

Fe05:
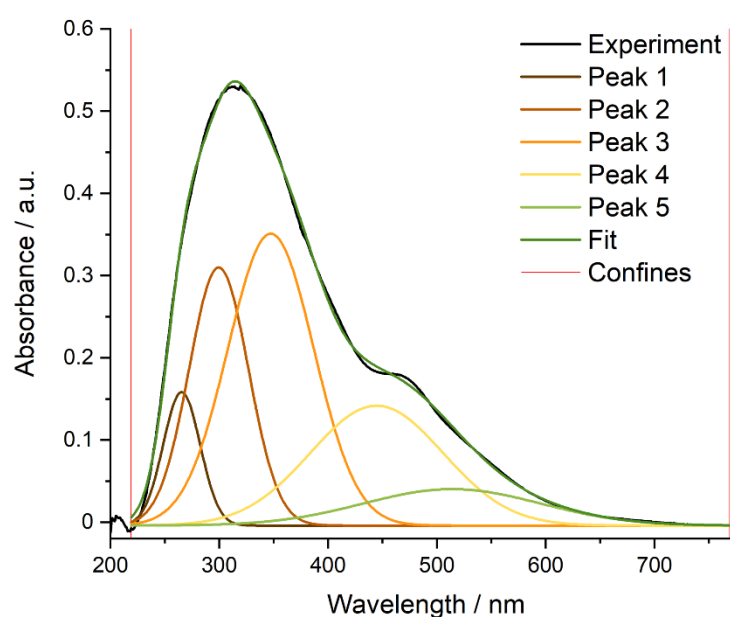
Figure S12: DRUV spectrum and deconvolution of Fe05.

Table S10: Parameters of the peak deconvolution of Fe05.

Model	Gaussian				
Function	y=y0 + (A/(w*sqrt(pi/2)))*exp(-2*((x-xc)/w)^2)				
	Peak 1	Peak 2	Peak 3	Peak 4	Peak 5
Y0	-0.004 ± 0.00147	-0.004 ± 0.00147	-0.004 ± 0.00147	-0.004 ± 0.00147	-0.004 ± 0.00147
x_c	265.51099 ± 0.77465	299.59546 ± 1.55765	347.44616 ± 8.9343	444.78092 ± 6.72789	513.93943 ± 334.27517
Area	6.9185 ± 2.22583	21.46817 ± 11.9875	35.09611 ± 14.23345	22.27018 ± 50.55156	9.01596 ± 47.92497
χ^2_{red}			1.85126E-5		
r^2_{corr}			0.9994		

Table S11: Assignment of the peaks and their normalized areas to tetrahedral, octahedral and oligomerized iron oxide. Percentual amounts of the respective iron species of the overall amount of catalyst, calculated from the percentual areas multiplied by the iron loading.

X_C [nm]	Area [a.u.]	Area$_{norm}$ [%]	Area$_{norm}$ [%]		Amount$_{norm}$ [wt%]
266	6.92	7.30111838	Fe$_{tet}$	7.30	0.36506
300	21.47	22.6524583	Fe$_{oct}$	22.7	1.13262
347	35.1	37.0331294	Fe$_x$O$_y$ olig.	60.5	3.02648
445	22.27	23.4965183			
514	9.02	9.51677569	Fe$_x$O$_y$ particles	9.52	0.47584
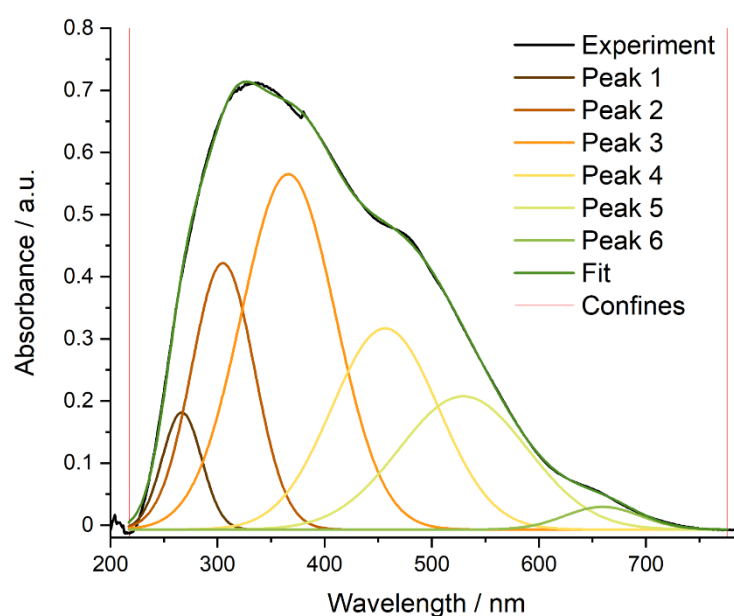
Fe10:

Figure S13: DRUV spectrum and deconvolution of Fe10.

Table S12: Parameters of the peak deconvolution of Fe10.

Model	Gaussian					
Function	$y=y0 + (A/(w*sqrt(pi/2)))*exp(-2*((x-xc)/w)^2)$					
	Peak 1	Peak 2	Peak 3	Peak 4	Peak 5	Peak 6
Y0	-0.007 ± 9.40638E-4	-0.007 ± 9.40638E-4	-0.007 ± 9.40638E-4	-0.007 ± 9.40638E-4	-0.007 ± 9.40638E-4	-0.007 ± 9.40638E-4
x_c	266.70925 ± 1.03707	305.05144 ± 1.38058	366.12353 ± 8.60039	456.49094 ± 37.17483	529.53263 ± 226.9542	659.49034 ± 10.0261
Area	8.71372 ± 2.6543	31.49412 ± 18.39082	62.94732 ± 51.60488	40.40586 ± 182.6243	32.19596 ± 151.95975	3.22821 ± 2.9828
χ^2_{red}	1.97494E-5					
r^2_{corr}	0.99971					

Table S13: Assignment of the peaks and their normalized areas to tetrahedral, octahedral and oligomerized iron oxide. Percentual amounts of the respective iron species of the overall amount of catalyst, calculated from the percentual areas multiplied by the iron loading.

X_C [nm]	Area [a.u.]	Area$_{norm}$ [%]	Area$_{norm}$ [%]		Amount$_{norm}$ [wt%]
267	8.71	4.86619364	Fe$_{tet}$	4.87	0.48662
305	31.49	17.5931616	Fe$_{oct}$	17.6	1.75932
366	62.95	35.1695625	Fe$_x$O$_y$ olig.	57.7	5.77462
456	40.41	22.5766803			
530	32.2	17.9898318	Fe$_x$O$_y$ particles	19.8	1.97944
659	3.23	1.80457009			

Fe20:
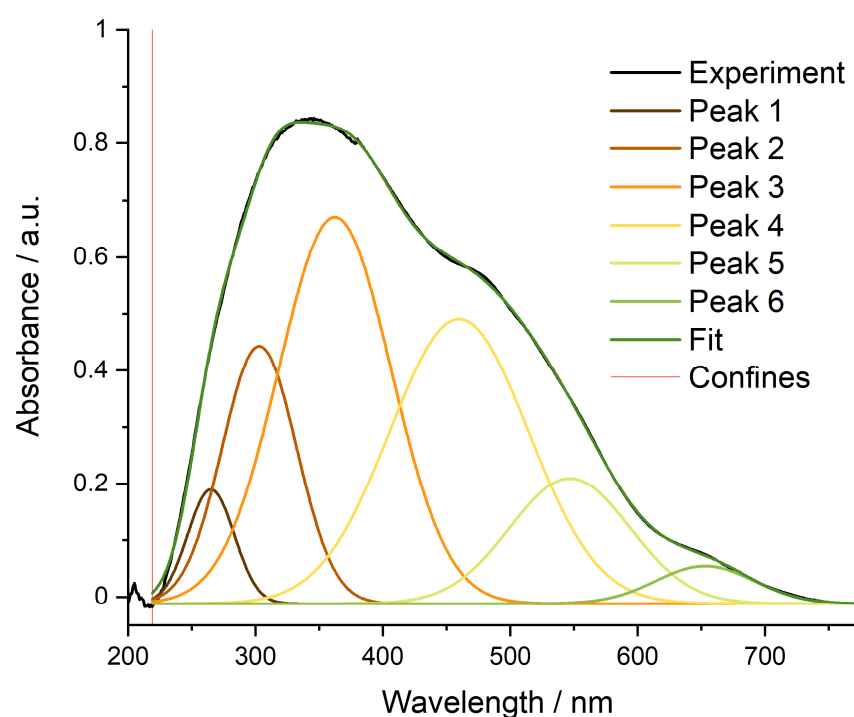
Figure S14: DRUV spectrum and deconvolution of Fe20.

Table S14: Parameters of the peak deconvolution of Fe20.

Model	Gaussian					
Function	$y=y0 + (A/(w*sqrt(pi/2)))*exp(-2*((x-xc)/w)^2)$					
	Peak 1	Peak 2	Peak 3	Peak 4	Peak 5	Peak 6
Y0	-0.012 ± 0.00103	-0.012 ± 0.00103	-0.012 ± 0.00103	-0.012 ± 0.00103	-0.012 ± 0.00103	-0.012 ± 0.00103
x_c	265.08132 ± 0.90556	303.06141 ± 1.18127	362.35649 ± 6.28092	459.83286 ± 15.1712	546.8148 ± 39.84401	652.81549 ± 5.69897
Area	9.21287 ± 2.50049	33.33717 ± 15.77893	75.51647 ± 43.38576	68.4914 ± 72.79266	26.18515 ± 44.30672	6.40267 ± 1.35892
χ^2_{red}	2.15064E-5					
r^2_{corr}	0.99976					

Table S15: Assignment of the peaks and their normalized areas to tetrahedral, octahedral and oligomerized iron oxide. Percentual amounts of the respective iron species of the overall amount of catalyst, calculated from the percentual areas multiplied by the iron loading.

X_C [nm]	Area [a.u.]	Area$_{norm}$ [%]	Area$_{norm}$ [%]		Amount$_{norm}$ [wt%]
265	9.21	4.20260096	Fe_{tet}	4.20	0.84052
303	33.3	15.2133242	Fe_{oct}	15.2	3.04266
362	75.5	34.4604152	Fe_xO_y olig.	65.7	13.1426
460	68.5	31.2525667			
547	26.2	11.9507187	Fe_xO_y particles	14.9	2.97422
653	6.40	2.92037417			

7. X-Ray Absorption Spectroscopy

Prepeak Analysis: Fe01 - Fe20

For prepeak analysis the main edge was subtracted as a Boltzmann-type function. To obtain the precise prepeak position an inverse polynomial function was applied for catalysts Fe01, Fe025, Fe05, Fe10 and Fe20 while for the references α-Fe$_2$O$_3$ and γ-Fe$_2$O$_3$ two Lorentzian functions were applied.
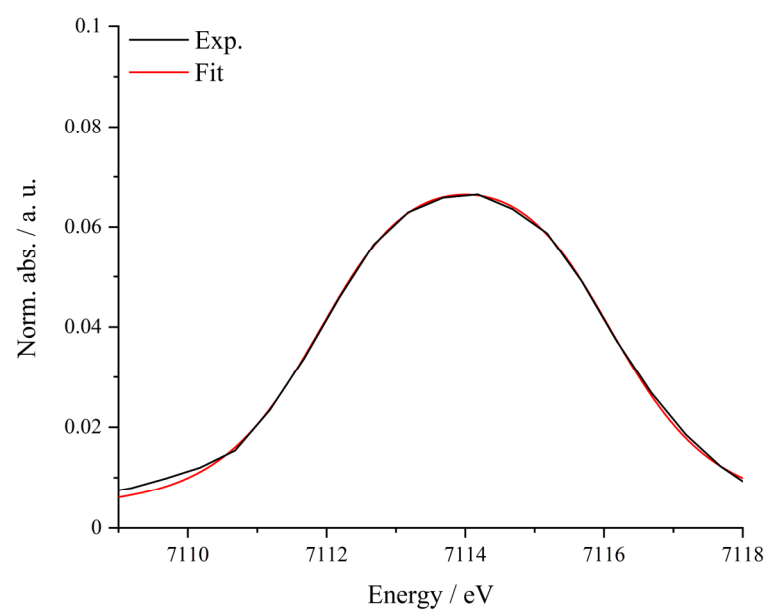
Fe01:
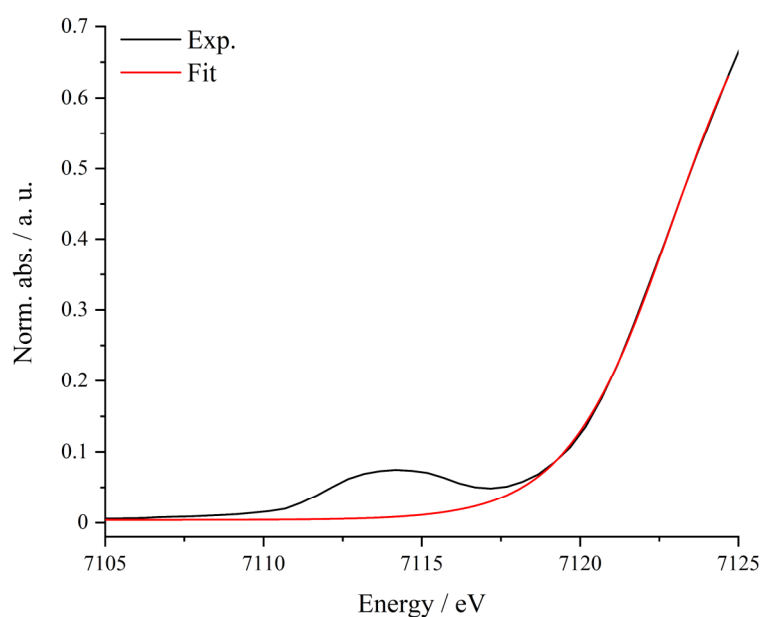
Figure S15: Prepeak area of Fe01 and the background to remove the main edge, obtained by a Boltzmann function.

Table S16: Fit parameters of the background fit for Fe01.

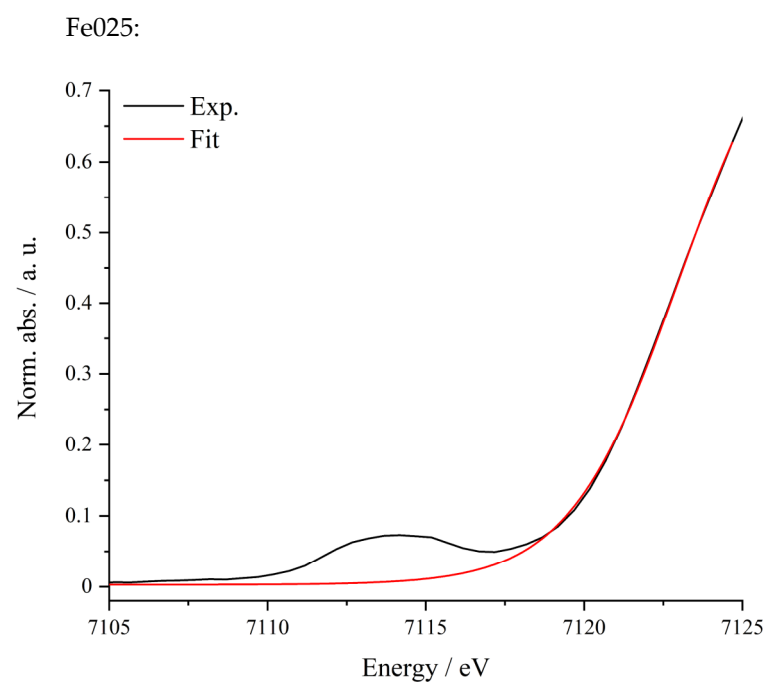| Model	Boltzmann
Equation	y = A2 + (A1-A2)/(1 + exp((x-x0)/dx))
Plot	Fe01
A1	0.00386 ± 5.57691E-4
A2	0.84933 ± 0.01596
x0	7122.92897 ± 0.07218
dx	1.671 ± 0.02862
χ^2_{red}	1.2797E-5
r^2_{COD}	0.99952
r^2_{corr}	0.99949

Figure S16: Prepeak area of Fe01 with inverse polynomial fit after removal of the main edge.

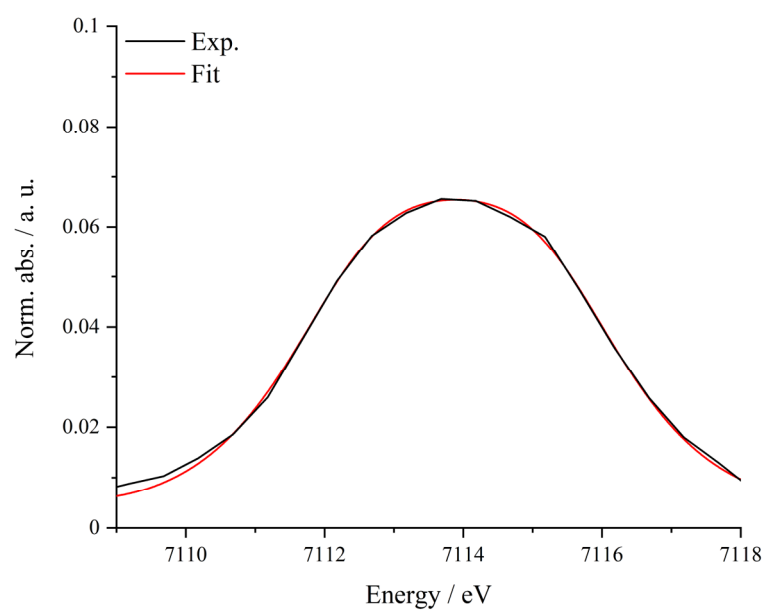**Table S17:** Fit parameters of the prepeak fit for Fe01.

Model	InvsPoly
Equation	y=y0+A/(1 + A1*(2*(x-xc)/w)^2 + A2*(2*(x-xc)/w)^4 + A3*(2*(x-xc)/w)^6)
Plot	Fe01
y0	0.00328 ± 0.00117
xc	7113.997 ± 0.02694
w	4.91615 ± 3842539.08757
A	0.06328 ± 0.00147
A1	0.50915 ± 795920.44293
A2	0.56888 ± 1778571.15333
A3	0.19565 ± 917539.61378
χ^2_{rd}	2.96405E-6
r^2_{COD}	0.99601
r^2_{corr}	0.99469

Fe025:

Figure S17: Prepeak area of Fe025 and the background to remove the main edge, obtained by a Boltzmann function.

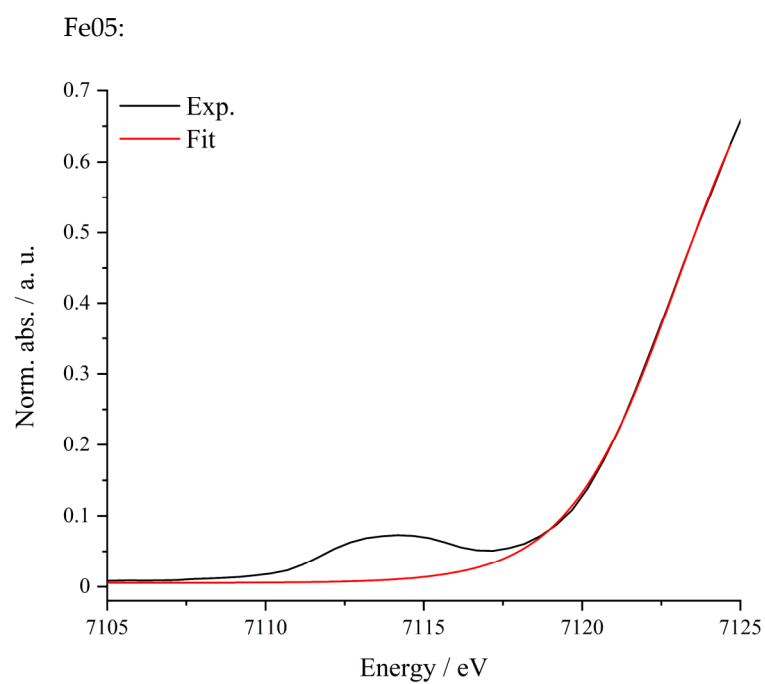**Table S18:** Fit parameters of the background fit for Fe025.

Model	Boltzmann
Equation	y = A2 + (A1-A2)/(1 + exp((x-x0)/dx))
Plot	Fe025
A1	0.00273 ± 7.69022E-4
A2	0.86027 ± 0.02297
x0	7122.97922 ± 0.10451
dx	1.72551 ± 0.03988
χ^2_{re}	2.43738E-5
r^2_{COD}	0.99907
r^2_{corr}	0.99902

Figure S18: Prepeak area of Fe025 with inverse polynomial fit after removal of the main edge.

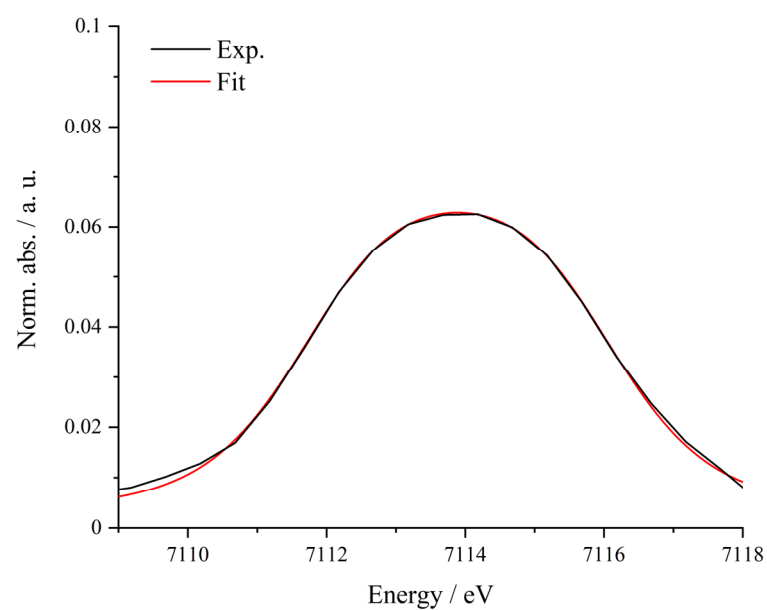**Table S19:** Fit parameters of the prepeak fit for Fe025.

Model	InvsPoly
Equation	y=y0+A/(1 + A1*(2*(x-xc)/w)^2 + A2*(2*(x-xc)/w)^4 + A3*(2*(x-xc)/w)^6)
Plot	Fe025
y0	-0.00433 ± 0.00603
xc	7113.8922 ± 0.02596
w	4.75552 ± 2515279.36997
A	0.06976 ± 0.00643
A1	0.30799 ± 325803.2086
A2	0.59565 ± 1260203.86425
A3	-0.0843 ± 267540.07923
χ^2_{ed}	2.60441E-6
r^2_{COD}	0.99645
r^2_{corr}	0.99493

Fe05:

Figure S19: Prepeak area of Fe05 and the background to remove the main edge, obtained by a Boltzmann function.

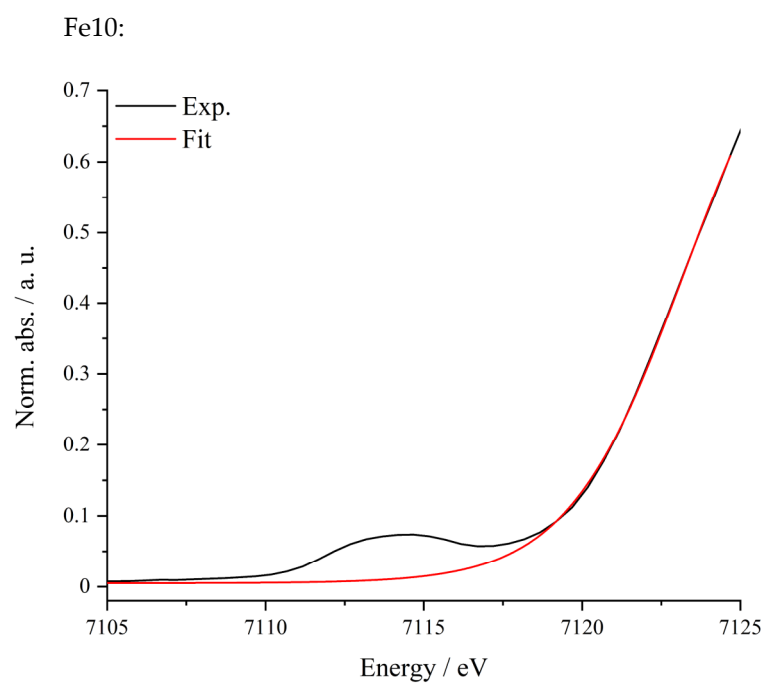**Table S20:** Fit parameters of the background fit for Fe05.

Model	Boltzmann
Equation	y = A2 + (A1-A2)/(1 + exp((x-x0)/dx))
Plot	Fe05
A1	0.00529 ± 6.10835E-4
A2	0.86658 ± 0.01905
x0	7123.05039 ± 0.08636
dx	1.74262 ± 0.03219
χ^2_{re}	1.5013E-5
r^2_{COD}	0.99942
r^2_{corr}	0.99939

Figure S20: Prepeak area of Fe05 with inverse polynomial fit after removal of the main edge.

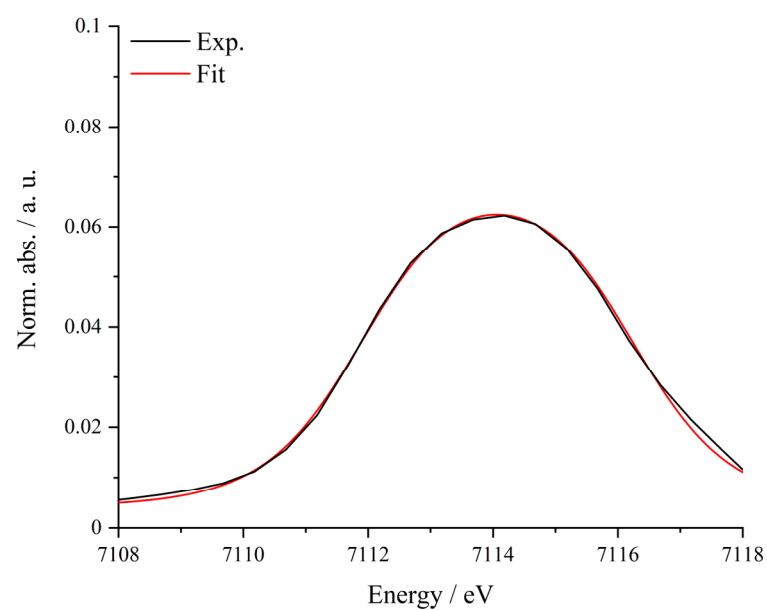**Table S21:** Fit parameters of the prepeak fit for Fe05.

Model	InvsPoly
Equation	y=y0+A/(1 + A1*(2*(x-xc)/w)^2 + A2*(2*(x-xc)/w)^4 + A3*(2*(x-xc)/w)^6)
Plot	Fe05
y0	0.00346 ± 0.00173
xc	7113.88537 ± 0.02625
w	4.59746 ± 3171995.4929
A	0.05939 ± 0.00178
A1	0.40488 ± 558690.86759
A2	0.41616 ± 1148502.29772
A3	0.11773 ± 487381.4119
χ^2_{red}	2.45021E-6
r^2_{COD}	0.99636
r^2_{corr}	0.99491

Fe10:

Figure S21: Prepeak area of Fe10 and the background to remove the main edge, obtained by a Boltzmann function.

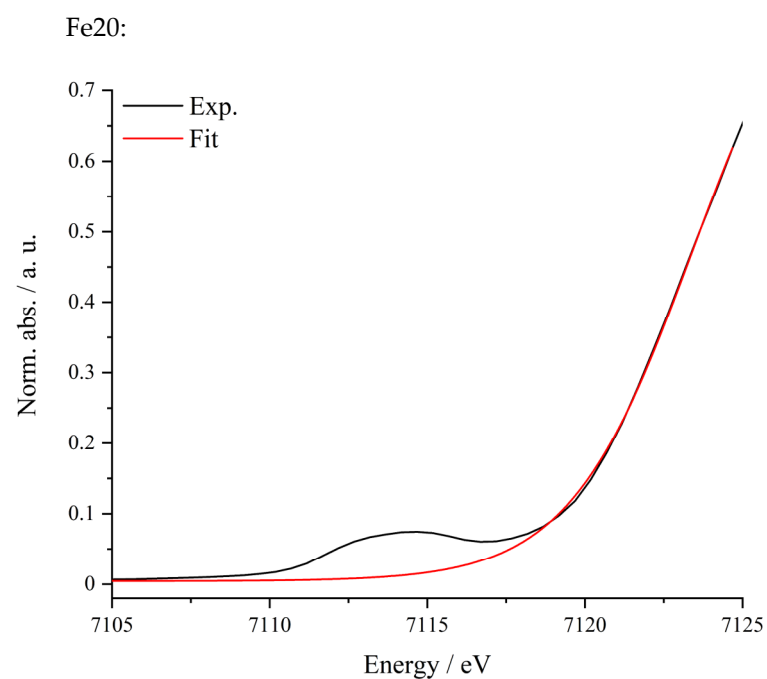**Table S22:** Fit parameters of the background fit for Fe10.

Model	Boltzmann
Equation	y = A2 + (A1-A2)/(1 + exp((x-x0)/dx))
Plot	Fe10
A1	0.00496 ± 6.03096E-4
A2	0.88208 ± 0.02301
x0	7123.22575 ± 0.10531
dx	1.83865 ± 0.03722
χ^2_{re}	1.49001E-5
r^2_{COD}	0.9994
r^2_{corr}	0.99936

Figure S22: Prepeak area of Fe10 with inverse polynomial fit after removal of the main edge.

Table S23: Fit parameters of the prepeak fit for Fe10.

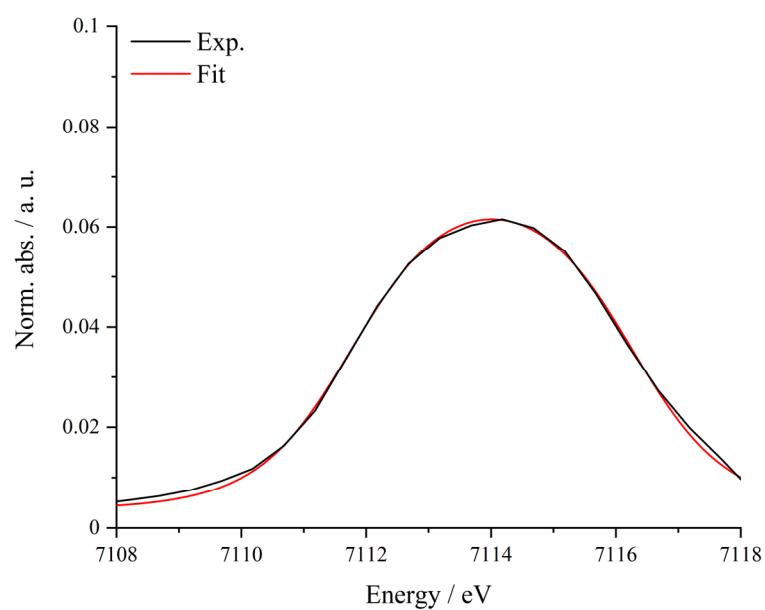| Model	InvsPoly
Equation	y=y0+A/(1 + A1*(2*(x-xc)/w)^2 + A2*(2*(x-xc)/w)^4 + A3*(2*(x-xc)/w)^6)
Plot	Fe10
y0	Fe10
xc	0.00648 ± 0.00725
w	7114.06544 ± 0.017
A	4.05682 ± 5774125.59664
A1	0.05577 ± 0.00704
A2	0.32289 ± 919147.83869
A3	0.30113 ± 1714388.62247
χ^2_{red}	0.05151 ± 439853.97278
r^2_{COD}	8.89577E-7
r^2_{corr}	0.99832

Fe20:

Figure S23: Prepeak area of Fe20 and the background to remove the main edge, obtained by a Boltzmann function.

Table S24: Fit parameters of the background fit for Fe20.

| Model	Boltzmann
Equation	y = A2 + (A1-A2)/(1 + exp((x-x0)/dx))
Plot	Fe20
A1	0.00435 ± 6.52698E-4
A2	0.93461 ± 0.02803
x0	7123.38387 ± 0.12485
dx	1.94507 ± 0.04109
χ^2_{red}	1.7425E-5
r^2_{COD}	0.99931
r^2_{corr}	0.99927

Figure S24: Prepeak area of Fe20 with inverse polynomial fit after removal of the main edge.

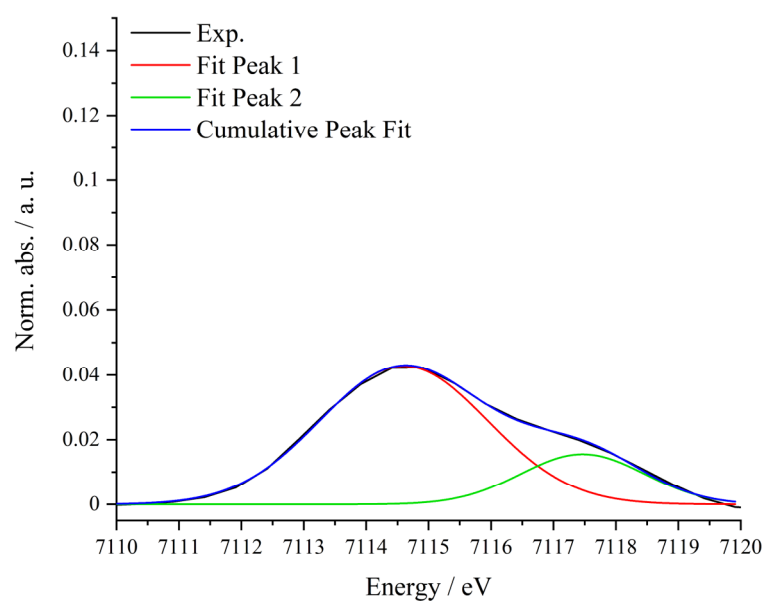**Table S25:** Fit parameters of the prepeak fit for Fe20.

Model	InvsPoly
Equation	y=y0+A/(1 + A1*(2*(x-xc)/w)^2 + A2*(2*(x-xc)/w)^4 + A3*(2*(x-xc)/w)^6)
Plot	Fe20
y0	$0.0035 \pm 8.78886E\text{-}4$
xc	7114.01046 ± 0.02646
w	$5.12845 \pm 3.9464E7$
A	0.05802 ± 0.00121
A1	0.5623 ± 8653906.19097
A2	$0.42336 \pm 1.30313E7$
A3	$0.28062 \pm 1.29566E7$
χ^2_{rd}	2.30855E-6
r^2_{COD}	0.99634
r^2_{corr}	0.99512
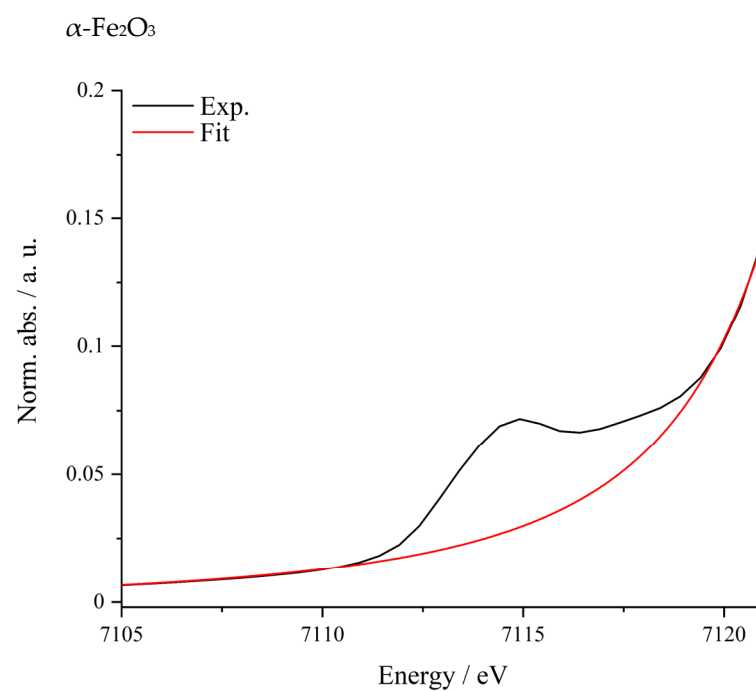
α-Fe$_2$O$_3$

Figure S25: Prepeak area of α-Fe$_2$O$_3$ at the Fe K-edge and the background to remove the main edge, obtained by a Lorentzian-type function.

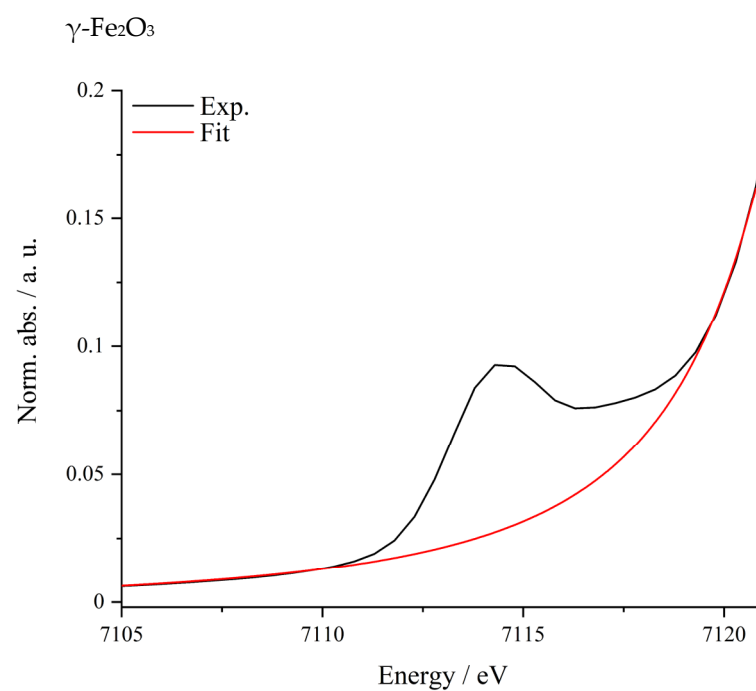**Table S26:** Fit parameters of the background fit for α-Fe$_2$O$_3$.

Model	Lorentz
Equation	y = y0 + (2*A/pi)*(w/(4*(x-xc)^2 + w^2))
y0	-0.00178 ± 6.17985E-4
xc	7125.08027 ± 0.59067
w	5.35235 ± 0.72219
A	4.0458 ± 1.05539
χ^2_{red}	3.41027E-7
r^2_{corr}	0.99979

Figure S26: Background-corrected prepeak of α-Fe$_2$O$_3$ and corresponding Gaussian-type peak fits and cumulative peak fit.

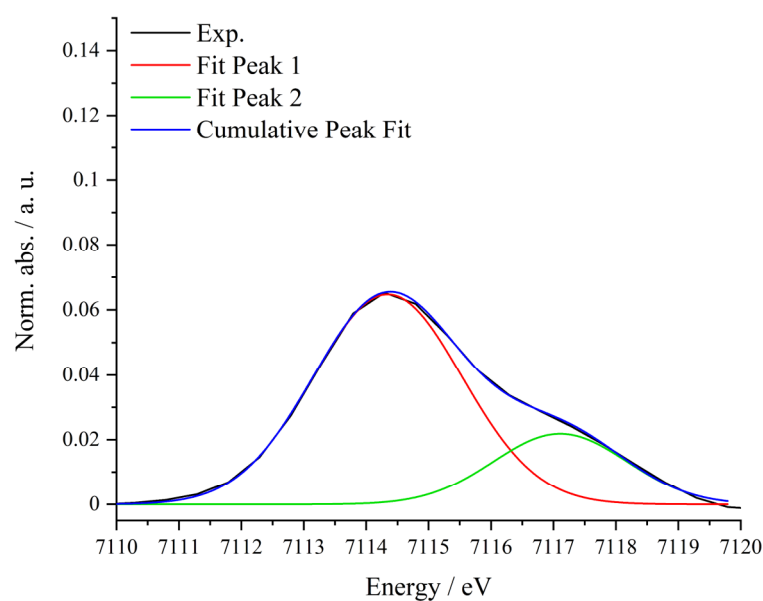**Table S27:** Fit parameters of the prepeak fit of α-Fe$_2$O$_3$.

Model	Gauss	
Equation	y=y0 + (A/(w*sqrt(pi/2)))*exp(-2*((x-xc)/w)^2)	
Plot	Peak1	Peak2
y0	0 ± 2.84616E-4	0 ± 2.84616E-4
xc	7114.60158 ± 0.03656	7117.46756 ± 0.0772
w	2.68567 ± 0.06306	1.98719 ± 0.10987
A	0.14395 ± 0.00405	0.03863 ± 0.00339
χ^2_{red}	3.6954E-7	
r^2_{corr}	0.99839	

γ-Fe₂O₃

Figure S27. Prepeak area of γ-Fe₂O₃ at the Fe K-edge and the background to remove the main edge, obtained by a Lorentzian-type function.

Table S28: Fit parameters of the background fit for γ-Fe₂O₃.

Model	Lorentz
Equation	y = y0 + (2*A/pi)*(w/(4*(x-xc)^2 + w^2))
y0	-0.00211 ± 6.79682E-4
xc	7124.56476 ± 0.56585
w	4.81389 ± 0.69828
A	4.28828 ± 1.19353
χ^2_{red}	4.27368E-7
r^2_{corr}	0.99981

Figure S28: Background-corrected prepeak of γ-Fe_2O_3 and corresponding Gaussian-type peak fits and cumulative peak fit.

Table S29: Fit parameters of the prepeak fit of γ-Fe_2O_3.

Model	Gauss	
Equation	y=y0 + (A/(w*sqrt(pi/2)))*exp(-2*((x-xc)/w)^2)	
Plot	Peak1	Peak2
y0	0 ± 3.00394E-4	0 ± 3.00394E-4
xc	7114.34287 ± 0.02922	7117.10866 ± 0.07861
w	2.39884 ± 0.04445	2.14073 ± 0.10752
A	0.19461 ± 0.00474	0.0586 ± 0.00441
χ^2_{red}	4.62017E-7	
r^2_{corr}	0.99908	

Prepeak and Edge Positions

Table S30: Prepeak and edge positions of Fe01 to Fe20 and the α- and γ-Fe_2O_3 references.

Catalyst	Pre-peak [eV]		Edge position [eV]
Fe01	7114.0		7126.0
Fe025	7113.9		7125.7
Fe05	7113.9		7125.4
Fe10	7114.1		7125.6
Fe20	7114.0		7125.4
α-Fe_2O_3	7114.6	7117.5	7125.1
γ-Fe_2O_3	7114.3	7117.1	7125.9

EXAFS Analysis (Fe01 - Fe20):
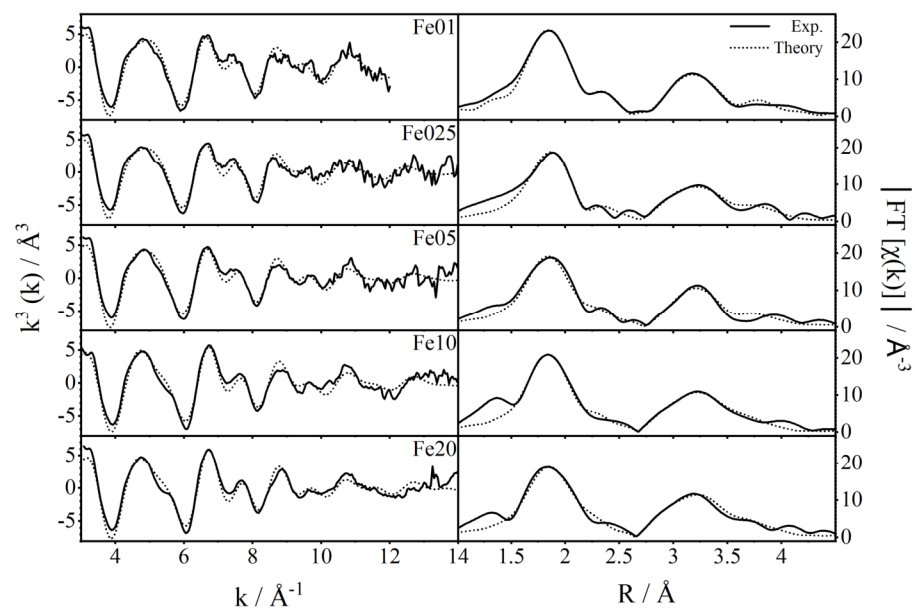
Figure S29: $k^3\chi(k)$ of the EXAFS spectra (left) and the corresponding Fourier transformed functions (right) of catalyst Fe01 to Fe20 and the fitted spectra.

8. Catalytic Activity

8.1. Catalysis Setup and Parameters

Catalytic experiments were conducted with 1 vol% CO (1.9 purity) in nitrogen (5.0), oxygen (4.5) and argon (5.0). The pressures were reduced by double stage reducing valves (GCE druva®) to a constant rate of 5 bar. The final gas mixture was set by mass flow controllers (ANALYT-MTC Messtechnik GmbH) to yield a lean composite of 1000 ppm CO and 10 vol% oxygen in inert gas with a total flow rate of 500 ml/min. The packed bed plug flow reactor was heated by a clamshell furnace (HORST GmbH, equipped with a JUMO dTron 304 controller) in a range of 200 mm (packed bed length approx. 10 mm) to ensure a uniform heating of the gas stream and the packed bed. The composition of the exhaust gas was analyzed by a NDIR analyzer (Infralyt 50, SAXON Junkalor® GmbH) equipped with two separate channels, one for carbon monoxide and one for carbon dioxide, both calibrated for a range of 0 to 1000 ppm.

8.2. Measurements at constant temperatures:

Fe01:
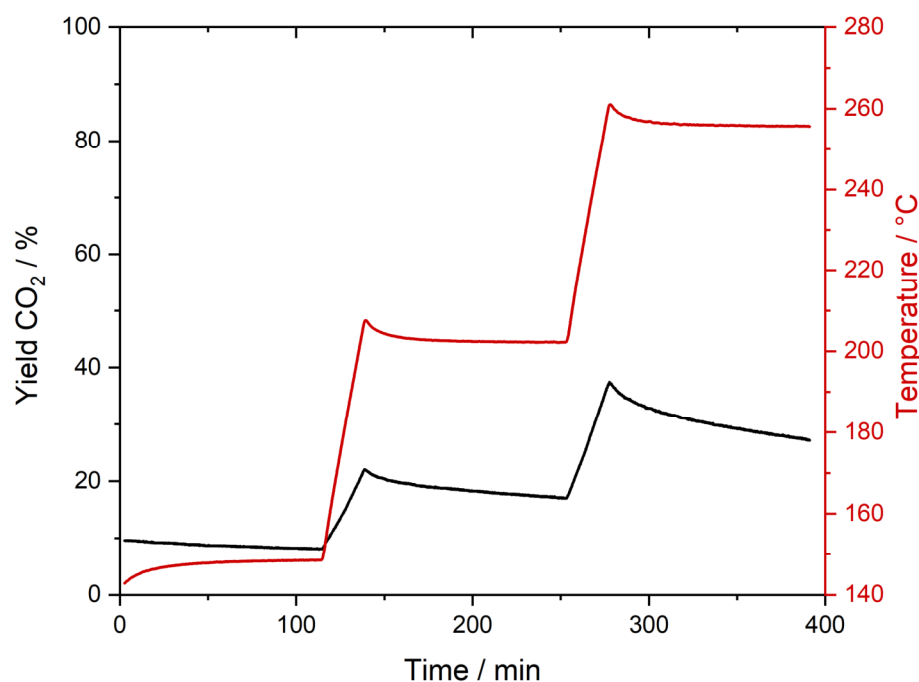
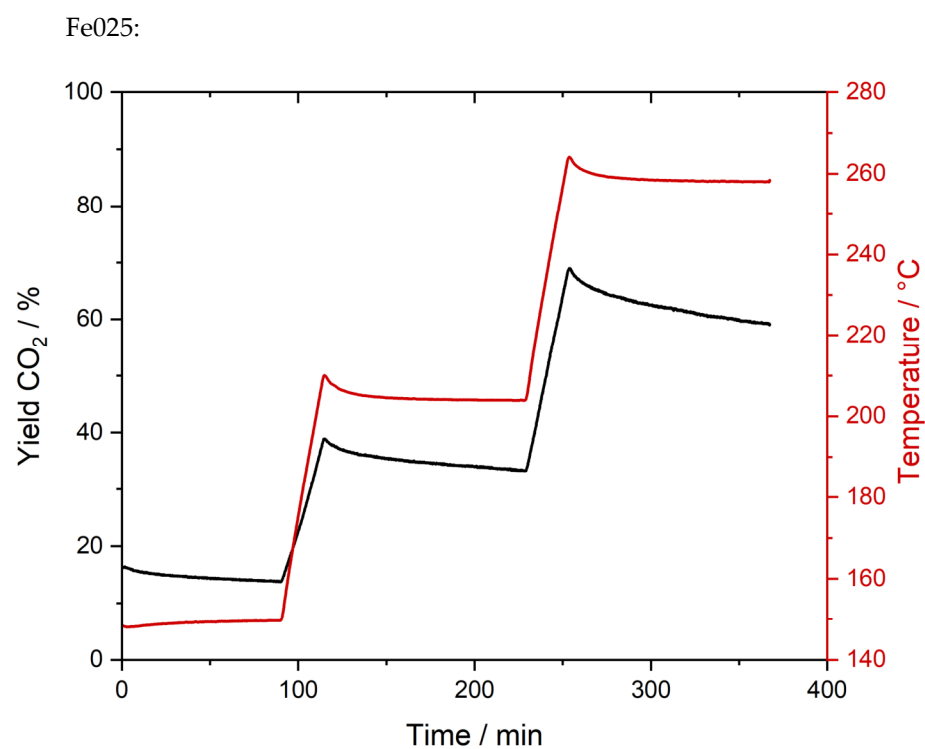**Figure S30:** CO oxidation experiment of Fe01 at constant temperatures.

Fe025:

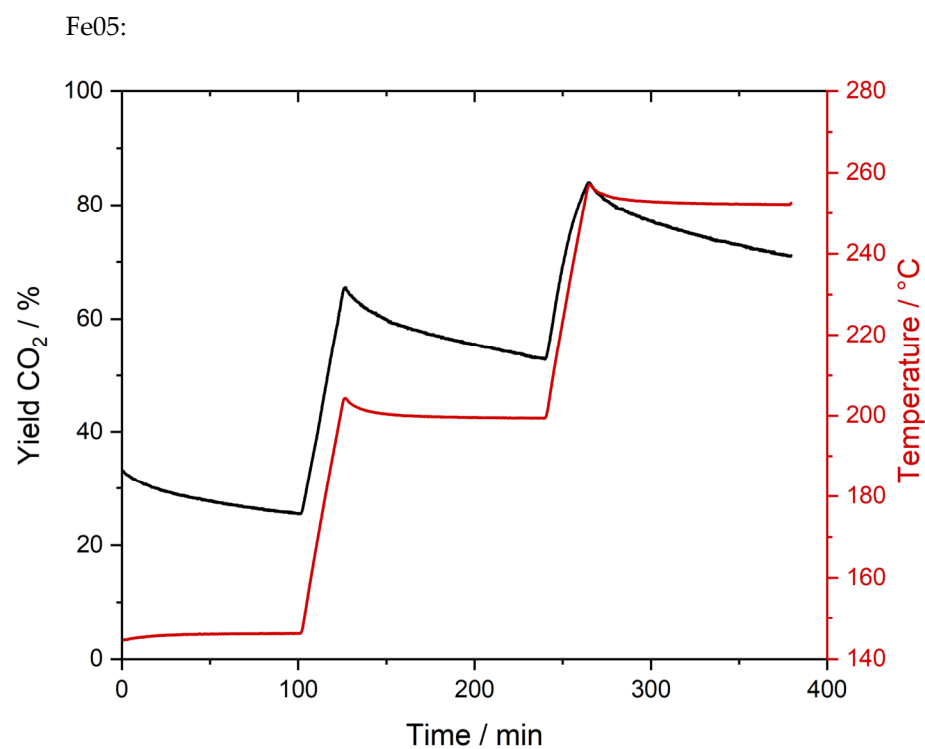**Figure S31:** CO oxidation experiment of Fe025 at constant temperatures.

Fe05:

Figure S32: CO oxidation experiment of Fe05 at constant temperatures.
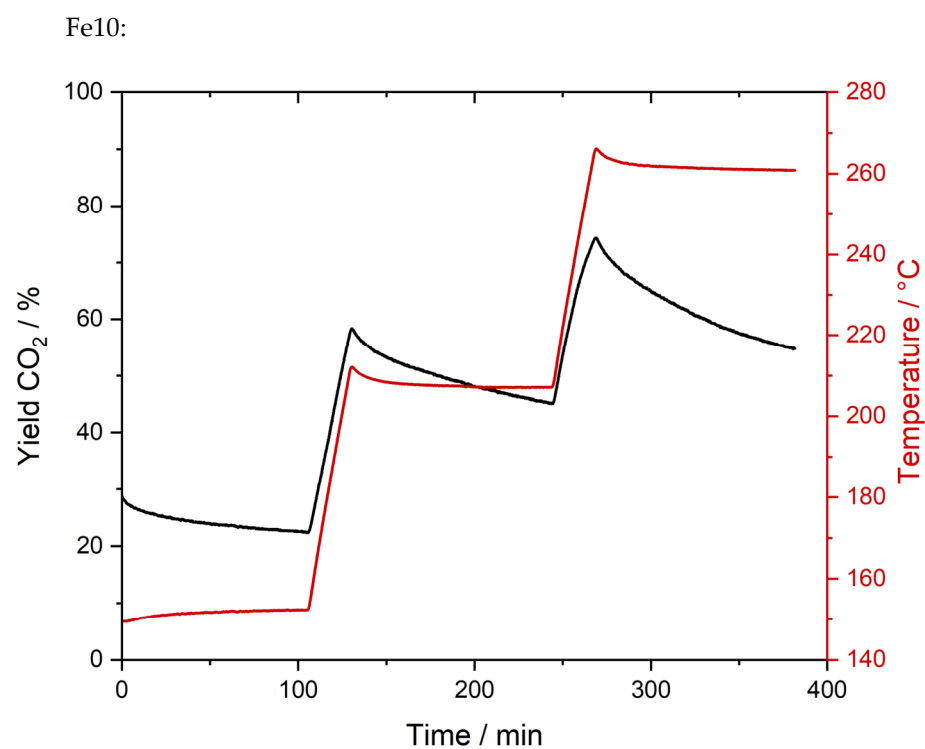
Fe10:

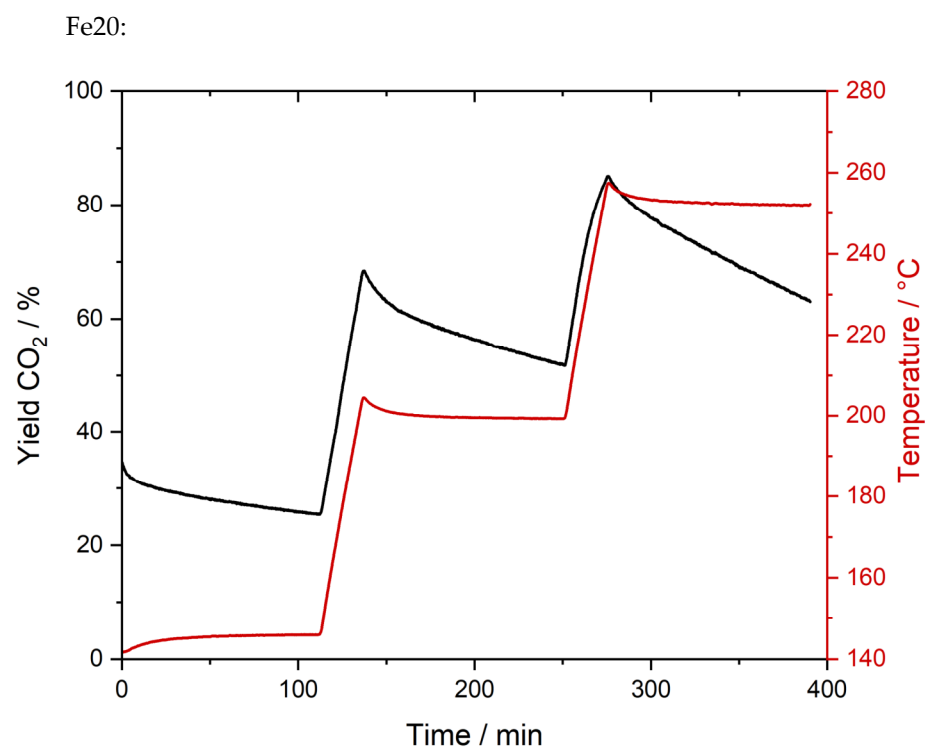**Figure S33:** CO oxidation experiment of Fe10 at constant temperatures.

Fe20:

Figure S34: CO oxidation experiment of Fe20 at constant temperatures.

References

1. Macrae, C.F.; Sovago, I.; Cottrell, S.J.; Galek, P.T.A.; McCabe, P.; Pidcock, E.; Platings, M.; Shields, G.P.; Stevens, J.S.; Towler, M.; et al. Mercury 4.0: from visualization to analysis, design and prediction. *J. Appl. Crystallogr.* **2020**, *53*, 226–235, doi:10.1107/S1600576719014092.
2. Gutiérrez, G.; Taga, A.; Johansson, B. Theoretical structure determination of γ−Al2O3. *Phys. Rev. B* **2001**, *65*, doi:10.1103/PhysRevB.65.012101.
3. Smrcok, L.; Langer, V.; Krestan, J. Gamma-alumina: a single-crystal X-ray diffraction study. *Acta Crystallogr., Sect. C: Cryst. Struct. Commun.* **2006**, *62*, i83-i84, doi:10.1107/S0108270106026850.